Article

Bull. Volcanol. Soc. Japan
Vol. 58 (2013) No. 1, pp. 163−181

Processes Prior to Outbursts of Vulcanian Eruption at Showa Crater of Sakurajima Volcano

Akihiko Yokoo[*,***], Masato Iguchi[**], Takeshi Tameguri[**] and Keigo Yamamoto[**]

(Received September 27, 2011; Accepted December 26, 2012)

Showa crater of Sakurajima volcano became active in June 2006 after 58 years of quiescence. From multi-parametric geophysical observations, we have identified the processes that typically occur prior to an explosive eruption at the crater. A few hours prior to the onset of an eruption, magma starts to migrate and accumulates at a depth of about 1 km. This accumulation of magma can be clearly observed in strain change records as an inflation process. Several tens of minutes prior to an eruption, the SO_2 gas emission rate gradually decreases, indicating that a sealing process is taking place in the crater bottom as the eruption nears. During the same time period, the volcano's inflation rate starts to accelerate due to the formation of a plug above the conduit that prevents the gas from escaping, with the result that a gas pocket forms beneath the crater. In nighttime events, a volcanic glow is also seen, which weakens and then disappears. A few minutes prior to an eruption, a small tremor starts to occur. Its amplitude grows as the strain changes from inflation to deflation as the stored gas is released through new fractures within the plug that had been confining the gas pocket, leading to a minor depressurization in the conduit. Then, an expansion process starts, that could explain seismically the first motion of an explosion earthquake. This is probably when the effect of depressurization downward from the crater bottom reaches the magma head and a sudden magma expansion with degassing starts. After a short period (about half a second), this expanding magma rises and pushes the gas pocket upward, leading to a swelling of the crater ground along with the radiation of the preceding phase of infrasound waves, and then a breakup occurs. After the plug fails due to deformation, the accumulated gasses and expanding magma are ejected together from the crater as the surface eruption phenomena starts.

Key words: Vulcanian eruption, eruption process, Sakurajima volcano, Showa crater

1. Introduction

Recent interdisciplinary and multi-parametric observations are attempting to elicit in detail the volcanic eruption processes at several active volcanoes including Stromboli, Italy (Calvari *et al.*, 2008) and Soufrière Hills, Montserrat (Voight and Sparks, 2010).

In Japan, Iguchi *et al*. (2008a) discussed the eruption process of the summit crater of Sakurajima volcano, based on integrated geophysical observations, as follows. The process commences with a gradual volcano inflation, which is thought to be induced by a combination of the effects of the ascent of magma and the accumulation of volcanic gas being emitted from the magma. Ishihara (1990) argued that such a gas accumulation leads to the formation of a "gas pocket" beneath the crater bottom. The term "gas pocket" corresponds to a shallow transition zone characterized by complex mingling between vesicular and dense magma a few hundred meters thick, which was mentioned as occurring at the Soufrière Hills volcano (Burgisser *et al.*, 2011). This zone is covered by a dense and strongly degassed plug a few tens of meters thick.

When the accumulated pressure inside the gas pocket exceeds the strength of the plug as gas accumulates, a failure of a tiny part of the plug, such as a fracture within it, may occur (Lyons *et al*., 2012). Then, a minor amount of gas will start escaping into the atmosphere. This leakage of gas induces a pressure decrease in the uppermost part of the conduit as well as within the gas pocket. It has been recognized in the strain change 1.5 min before an eruption (Iguchi *et al*., 2008a). The depressurization in the conduit can then propagate deeper into the volcano as an expansion wave (Turcotte *et al.*, 1990). When this happens, a sudden outgassing of water-saturated magma occurs at a certain depth, which corresponds to the onset of an explosion earthquake in the conduit around 2 km beneath Sakurajima (Ishihara, 1985; Tameguri *et al.*, 2002).

[*] Aso Volcanological Laboratory, Institute for Geothermal Science, Graduate School of Science, Kyoto University, Minami-Aso, Kumamoto 869−1404, Japan.
[**] Sakurajima Volcano Research Center, Disaster, Prevention Research Institute, Kyoto University, 1722−19, Sakurajima Yokoyamacho, Kagoshima 891−1419, Japan.

Corresponding author: Akihiko Yokoo
e-mail: yokoo@aso.vgs.kyoto-u.ac.jp

An additional process of expansion occurs at the top of the conduit (～0.5 km deep) 1 s after the onset of the explosion earthquake. During this second, a pressure wave is believed to propagate in the conduit from the source to the explosion earthquake to the shallow expansion source, at a propagation speed of 1.4−1.9 km/s (Tameguri *et al.*, 2002). This secondary effective expansion suggests that the gas pocket starts to push up both the plug (the bottom of the crater; Yokoo *et al*., 2009) and the rock of the conduit walls.

Upon the disruption of the plug, a strong air shock wave is radiated by release of the built-up gas pressure. The instantaneous (～1 s) opening of the crater bottom necessarily leads to an abrupt but shallow pressure decrease (strain-step; Ishihara, 1990). Simultaneously, a mixture of fragmented magma and volcanic gas starts to be emitted from the conduit as an eruption cloud. This causes the local ground deformation observed as volcano deflation.

Some geophysical and visual observations suggest the existence of a pressurized gas pocket (a highly viscous and highly pressurized region confined by a plug and the conduit walls) that disrupts at the time of eruption, indicating it was formed prior to the eruption. Pressure accumulation is thought to play an important role in precipitating the occurrence of an eruption (Burgisser *et al.*, 2011; Gottsmann *et al.*, 2011). However, there have not been sufficiently clear manifestations of evidence to allow us to understand the processes involved in the formation (and disruption) of a gas pocket with a correct time scale compared with the accumulation of the magma pressure. Although the storage of pressurized volcanic gas within the gas pocket prior to an explosive eruption necessarily induces gradual and relatively local inflation around the crater, we have not yet been able to uniquely identify this process in observed records of the summit crater eruptions. One possible reason for this is that geodetic records at commonly distant stations, without those at nearer dangerous stations, are more sensitive to the large inflation induced by deeper magmatic sources (apparently, magma migration itself) than to the tiny signals that stem from the gas accumulation process (Ishihara, 1990).

Basically similar processes are thought to occur during eruptions in the newer Showa crater of the Sakurajima volcano (the Showa crater is described in the next section). The aim of this paper is to present clear evidence that will help to elicit the dynamic processes of gas pocket regions, taking the Showa crater eruptions as an example. First, we describe the activity of the Showa crater in Section 2, and our observation network targeting Showa crater eruptions in Section 3. Next, we detail the shallow processes that take place prior to eruptions observed by the observation systems in Section 4, and finally, in Section 5, we discuss the entire eruption process and its dynamics in the Showa crater by making a comparison with eruptions of the summit crater.

2. Eruption activities at Sakurajima volcano

Sakurajima volcano, located in the southern part of Japan, is known for its repeated small, mild vulcanian eruptions (VEI 0−1). Numerous eruptions have occurred in the summit crater since 1955, and they are generally accompanied by strong air shocks, the ejection of volcanic bombs, and a large amount of volcanic material (Ishihara, 1985). The recorded amplitude of an air shock that occurred in the 1980s exceeded 500 Pa at the station, situated 2.7 km from the summit crater (HAR; Fig. 1a). At the same time, meter-sized volcanic blocks occasionally reached residential areas 2.5−3.5 km to the south of Sakurajima. The total mass of ash emitted from 1978 to 2000 amounts to approximately 2×10^8 tons (Ishihara, 2000). Another remarkable characteristic of Sakurajima vulcanian eruptions is a cyclic inflation-deflation pattern of ground deformation associated with each eruption (Ishihara, 1990; Iguchi *et al.*, 2008a). This cycle has come to be used to forecast eruptions as an inflationary radial tilt is observed for periods of 10 min to 7 h prior to eruptions, enabling automated warnings to be issued (Kamo and Ishihara, 1989).

Although the total number of explosive eruptions had reached 7902 at the end of 2009 (Fig. 2), eruption activity at the summit crater suddenly abated in 2003. Only a few explosions per year have been observed since then. In contrast, in June 2006, the Showa crater on the eastern flank of Sakurajima reactivated after a 58-year silence (Yokoo *et al.*, 2007; Yokoo, 2009) (Fig. 1). Eruption activity in the Showa crater is thought likely to have replaced activity in the summit crater in recent years (Fig. 2).

The initial reactivations at the Showa crater in 2006 and 2007 were relatively minor, with only intermittent small emissions of ash accompanied by ash clouds a few hundred meters high. The activity has gradually become much more vigorous since 2008, and eruption clouds have risen to a height of 1−4 km above the crater. Pyroclastic density currents (PDC) have sometimes been observed reaching ＜1.5 km from the crater (Figs. 1b and 1c). The diameter of the crater is also gradually growing, reaching about 300 m in March 2010. The annual number of explosive eruptions at the Showa crater reached 984 at the end of November 2010 (Fig. 2). This number of events is double the maximum number at the summit crater in 1974 (489 events), although the scale of the eruptions at the Showa crater is much smaller than the summit crater eruptions in the 1970s to the 1980s (Iguchi *et al.*, 2010).

3. Observation network

The Sakurajima Volcano Research Center (SVRC) of Kyoto University has installed a multi-parametric observation network around Sakurajima volcano, spurred by the recurrence of eruptions from the Showa crater. Fig. 1a shows SVRC's permanent stations.

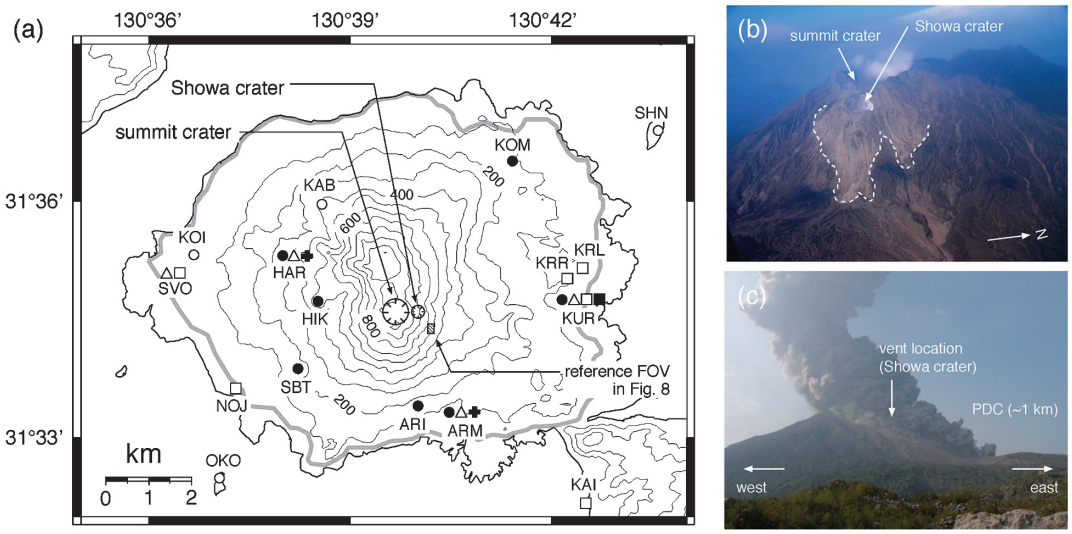

Fig. 1. (a) Observation network at Sakurajima volcano. The four open and seven closed circles denote short-period and broadband seismometer stations, respectively. The four triangles indicate stations equipped with infrasound sensors. Video cameras are set up at the six stations shown by open squares. Four of them, NOJ, KAI, KRR, and KRL, are operated by the Japanese Ministry of Land, Infrastructure, Transport and Tourism. KUR is also equipped with an infrared thermal camera (closed square). Tiltmeters and extensometers are installed in underground tunnels at both HAR and ARM (crosses). The thick gray line along the coast denotes the route of traverse measurements of SO_2 emission rate. The hatched area on the southeastern flank of the volcano is the reference region of Fig. 8. (b) Aerial photograph around the southeastern flank of Sakurajima taken on April 10, 2009, with the support of Kagoshima Prefecture. The light-colored area around the Showa crater, surrounded by a broken line, is covered with deposits from pyroclastic density currents (PDC) from the day before the aerial photography flight. (c) An eruption of Showa crater on April 9, 2009, showing a dense PDC covering a distance of about 1 km. This photograph was taken from a position near ARM.

At opposite sides of the volcano (ARM and HAR), two-component water-tube tiltmeters and three-component extensometers constructed from super inver-bars have been installed in underground tunnels. The signals from these sensors are sampled at 1 Hz. As the ground tilt and strain records at both stations are generally synchronized with variations in sea level, as already reported by Ishihara (1990), both records are corrected using BAYTAP-G (Tamura *et al.*, 1991) and the actual tides recorded at the southern part of Sakurajima, as noted in Tateo and Iguchi (2009). Note that ARM is operated by the Japanese Ministry of Land, Infrastructure, Transport and Tourism (MLIT) working in collaboration with SVRC.

Visual and infrared thermal cameras (operating at 30 fps and 1 fps, respectively) have been deployed at two stations—SVO and KUR (Yokoo, 2009; Yokoo *et al.*, 2009) — and are synchronized by a GPS clock. MLIT has also established a video monitoring network with high-sensitivity TV cameras and infrared thermal cameras. Images from some of these cameras are freely available via the Internet[1], with time delays of between 0.5 min and 2 min caused by encoding/decoding procedures and network traffic. Movies from the MLIT cameras are saved at SVO at 1-min intervals and the time is corrected by making a comparison with our own movie records.

Short-period three-component seismometers have been installed at 11 seismic stations. Eight of these seismometers are sited in boreholes, and the others are on the ground surface (Tameguri *et al.*, 2002). Seven stations of the short-period seismometer are also equipped with broadband seismometers. To detect infrasound waves, low-frequency microphones have been set up at four stations. Seismic and infrasound data are logged at 200 Hz, apart from at KUR station where infrasound is logged at 100 Hz (Fig. 1a).

Additionally, measurements of the SO_2 gas discharge rate are occasionally conducted using miniature UV spectrometers (Mori *et al.*, 2007) mounted on a vehicle driven along a road that circles the volcano near the coastline (Fig. 1a). These SO_2 measurements were taken roughly once a week in 2008 (62 observations), once every 2.5 weeks in 2009 (20 observations), and once a month in 2010 (11 observations). Fewer observations were made in

[1] http: //www. qsr. mlit. go. jp/osumi/camera_sabo. htm (in Japanese)

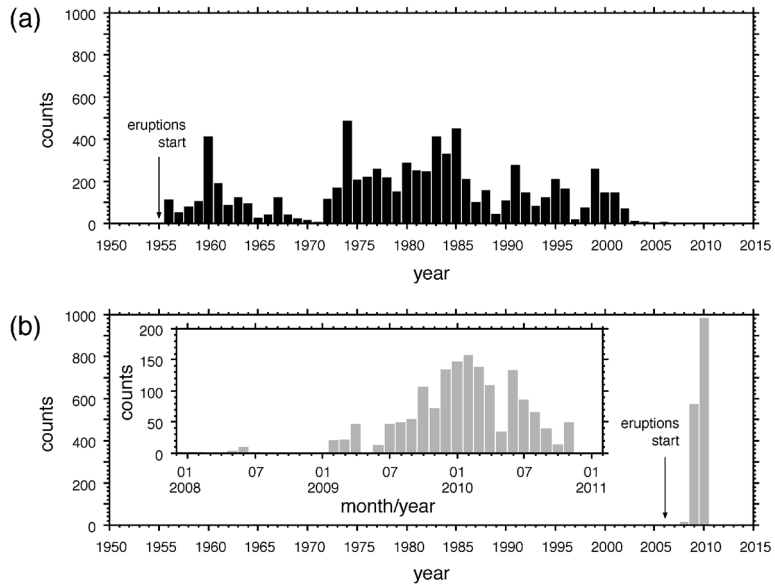

Fig. 2. Annual numbers of explosive eruptions accompanying large infrasound waves occurring at (a) the summit crater (＞10 Pa at HAR or ＞5 Pa at SVO) and (b) Showa crater (＞10 Pa at ARM). The inset diagram in (b) shows the monthly numbers of Showa crater eruptions. The data cover eruptions counted until the end of November, 2010.

2009 and 2010—despite the increasing eruption activity (Fig. 2) —because we choose to make observations when conditions are favorable for DOAS (fair skies, strong winds, and no ash dispersion in the air) to reduce errors in the SO_2 estimation.

4. Recorded signals

The results of our multi-parametric observations are summarized in Table 1, with details provided below.

4−1 Prior to eruption

Ground deformation

The tilt and strain changes that accompanied the cyclic vulcanian eruptions over three days in August 2009 are shown in Fig. 3. They were recorded in the underground tunnel at ARM (Fig. 1a), 2.3 km from the Showa crater. Although they were corrected as described in the previous section, the radial and tangential tilt changes still have relatively large fluctuations of 40−60 nano-radians within a half-day period (Fig. 3a) caused by tidal effects. Although tilt changes corresponding to each eruption are identified the same as for summit eruptions (Ishihara, 1990), the changes —especially in the expected inflation stage (20−90 nrad/h at the summit eruptions; Tateo and Iguchi, 2009) — prior to the onset of each eruption are not identified.

As opposed to the tilt record, characteristic strain changes prior to the occurrence of each eruption are clearly recognizable (Fig. 3b). For instance, the radial component shows a 48 nano-strain contraction starting 6.5 h prior to an eruption at 09 : 52 on August 6, 2009, while the tangential component shows an extension of around 39 nano-strains. At the onset of the eruption, an inverse trend is recorded in both components; that is, the radial and tangential strains show a rapid extension and contraction, respectively. Such patterns of inverting the trend in the tilt, and also in the strain at HAR, sited 3. 1 km in a horizontal direction on the opposite side of the volcano (Fig. 1a), are smaller than for ARM. The geodetic signals at HAR may be obscured not only by the distance, but also by the complicated topography between the Showa crater and the station, which includes the summit crater with a depth ＞500 m.

Here we categorize typical patterns of strain change prior to an eruption into the three stages.

i) 1st Stage

A radial contraction and tangential extension prior to the onset of an eruption is generally observed (Fig. 3b). However, the duration is quite different for each vulcanian eruption event. The average duration of the signals ranged between 4 and 16 h in May 2008 (Iguchi *et al.*, 2008b), but in December 2009, it decreased to only a few tens of minutes to 1.5 h. In some cases, a very complicated strain change, consisting of a contractions-and-extensions pattern in the two components, followed by a hiatus lasting 10 min to 3 h prior to the eruptions, were recognized. During this period, no surface phenomenon such as ash emission was visible in the movie records contrary to the case at the summit crater where ash emission was observed during

Table 1. Summary of observation results of processes leading to a Showa crater eruption.

	prior to eruption			at the time of eruption	frequency*
	1st stage	2nd stage	3rd stage		
ground deforamtion (strain)	extention in radial comp. contraction in tangential comp.				◎
		accelerating (radial: ext., tangential: cont.)			○
			inverting (radial: cont., tangential: ext.)		◎
seismogram	small earthquakes				△
			increas in tremor amplitude		○
				explosion earthquake	◎
infrasound				preceding and main phases	◎
video record		glow disappearance			△
infrared movie			temperature increase		×
SO_2 release		decreasing			×
time scale**	a few hours	a few tens minutes - a few minutes	a few minutes		
interpretaiton	discussed in 5.1	5.2	5.3	5.4	

* frequency of the phenomenon is categorized into 4 levels; ◎: generally observed, ○: frequently observed, △: sometimes observed, ×: occasionally observed.

** prior to eruptions

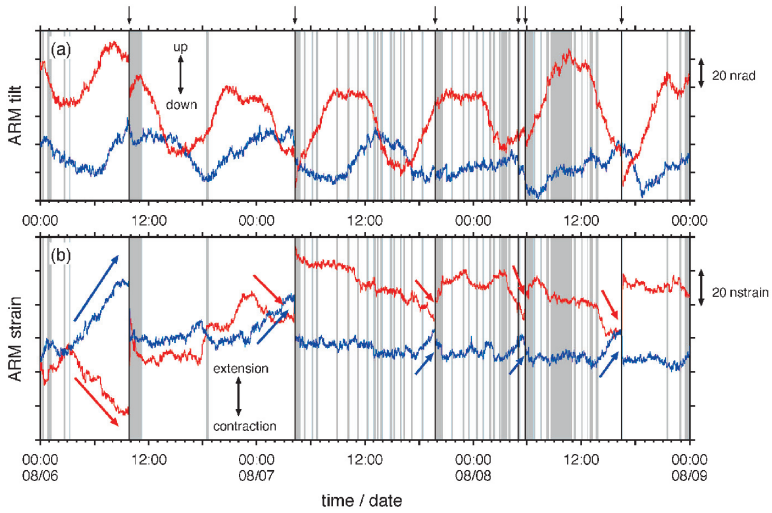

Fig. 3. Tilt and strain records at ARM during a 3-day period from August 6 to 9, 2009. Six thin vertical black lines with arrows at the top of the diagram indicate the onset times of major eruptions counted routinely for Fig. 2. Numerous gray-colored periods denote periods of ash venting from the crater. (a) Tilt change of radial and tangential components with respect to the crater (red and blue lines, respectively). (b) Strain changes of radial (red) and tangential (blue) components. Preparing patterns toward the next eruption are clearly identified for both components as indicated by the set of thick arrows.

"suspension process in tilt" (Tateo and Iguchi, 2009). In addition, no gas emissions were observed during those periods.

ii) 2nd Stage

The rate of strain change increased slightly from a few tens of minutes to a few minutes prior to the onset of an eruption (Fig. 4). The amplitudes of the rate changes were not much larger than those of regular fluctuations in the strain records (a few nano-straions; see Appendix), thus it was difficult to determine the period of this stage correctly from only the strain data. However, the period of an increased rate of strain change coincided with various surface phenomena at the crater, as described later.

iii) 3rd Stage

A few minutes prior to the onset of an eruption, the pattern of ground deformation inverted from contractions to extensions in radial strain, and from extensions to contractions in tangential strain (Fig. 5a). Fig. 5b shows a histogram of the time differences between the timing of this strain change and the onset of an eruption estimated for 179 events recorded between August and September 2009. There is a clear unimodal time difference peak a few minutes prior to an eruption ($>$81.6% from 0−5 min).

Seismograms

During the 1st stage periods of strain records, small earthquakes were sometimes observed at HIK, one of the nearest seismic stations to the Showa crater (2.2 km; Fig. 1a). Fig. 6 shows an example of such an earthquake sequence prior to the 01:15 eruption recorded on August 23, 2009. In this case, a few minutes after ash stopped venting from the crater (21:38−22:37), a multitude of small earthquakes started at 22:39, averaging one event every 3.5 min (circles in Fig. 6). The spectral peak of these earthquakes was of 3−8 Hz, so they are classified as "BH-type" earthquakes (Iguchi, 1995) in Sakurajima. Because of their small amplitudes ($<10\mu$m/s at HIK), they were hardly recorded at the other seismic stations except for ARM. This makes it impossible to determine their source locations, depths, and mechanisms.

Fig. 7 shows the vertical component of the velocity seismogram at HIK (Fig. 1a) and raw extensometer data (the radial component at ARM) for the eruption on September 27, 2009. There was a tremor starting at 01:38:02, about 1.5 min prior to the eruption, and its amplitude started to increase at around 01:38:25. The change in the trend of ground deformation (that is, the 3rd stage of the strain record) seems to start at the same time (vertical dashed line in Fig. 7). The spectral peak of these tremors was around 4 Hz or less.

Video records

A volcanic glow was sometimes seen at night in the middle of 2009. As shown in Fig. 8a, a strong volcanic glow emerged just above the crater at 02:43 on August 27, 2009. That glow weakened gradually and disappeared (02:57), and 2 minutes after, at 02:59, an eruption rich in incandescent blocks occurred.

We obtain the time series of the changing glow strength by using the R-channel values (8 bit; 0−255) of the RGB

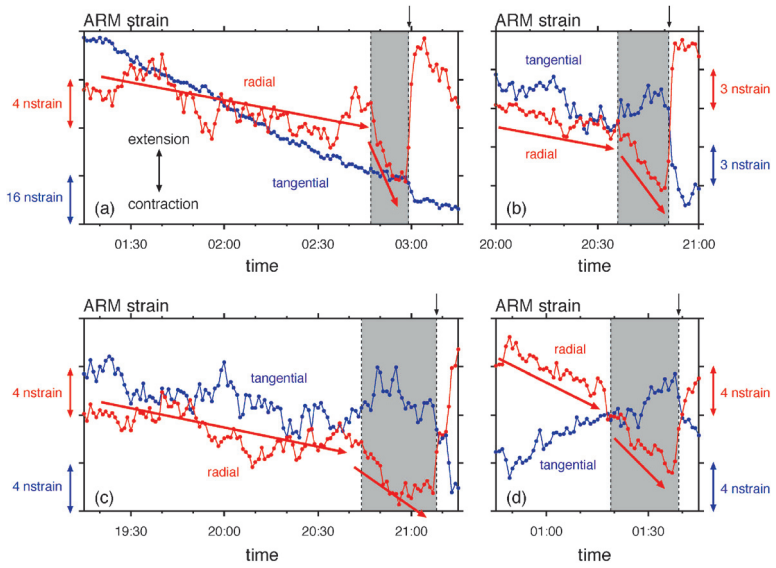

Fig. 4. Strain changes recorded at ARM on (a) August 27, (b) August 28, (c) September 2, and (d) September 27, 2009. Shaded periods denote the times of weakening and then disappearance of a volcanic glow (Fig. 8). The broken vertical lines with black arrows on the right denote the onsets of the eruptions. Thick arrows show the trend in changes of the radial component. Note that the tangential record is disordered as a contractive trend, in particular in (a), but it also shows a changing trend.

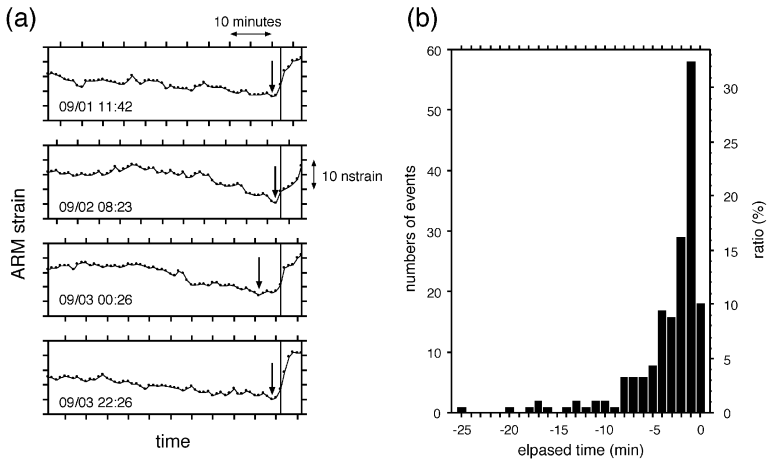

Fig. 5. (a) Four examples of radial strain observed at ARM. The arrows represents the time when the strain changed to the inverse direction, while the eruption occurred at the time shown by the thin vertical line. (b) Histogram of time difference between the strain change and the onset of an eruption between August and September 2009 (179 events).

color scale for two selected fields of view ("glow 1" and "glow 2" FOVs) in the movie imagery (Fig. 8a). "Reference" FOV on the southeastern flank of the volcano is taken as the reference region for the color measurement. The corresponding area of the reference FOV is shown in Fig. 1. Increases and decreases in the R-values indicate a strengthening or weakening in the reddish color on the digital images, respectively.

At 02:47 (12 min prior to the onset of the eruption), the average R-values in the "glow 1" and "glow 2" FOV regions started to decrease from around 250 to 140, reaching almost the same values as the "reference" FOV region at 02:53 (6 minutes elapsed time) (Fig. 8b). The R-value in the "reference" FOV was stable at 135 prior to the

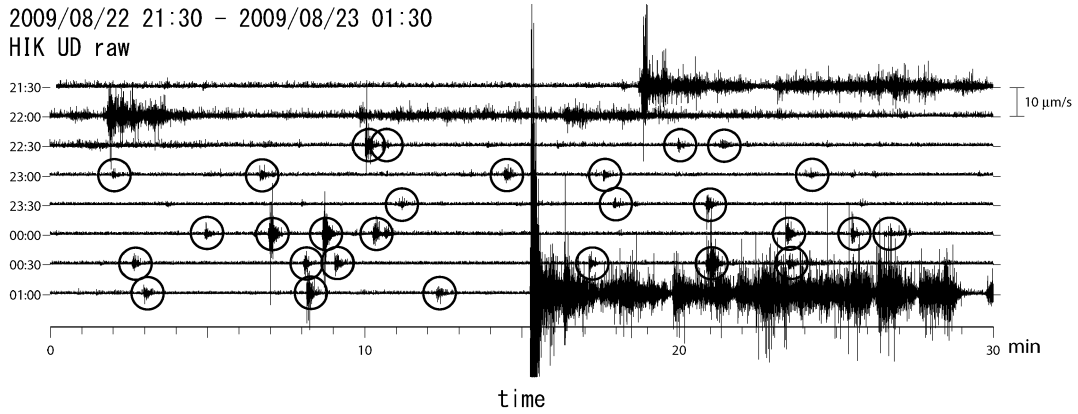

Fig. 6. Seismogram of the vertical component at the station HIK lasting 3.5 h from 21 : 30 on August 22, 2009. After the first BH-type earthquake (Iguchi, 1995) started around 22 : 40, many small earthquakes, marked by circles, occurred as the 01 : 15 eruption approached. Note that ash was ejected from the Showa crater during the period of 21 : 48–22 : 37.

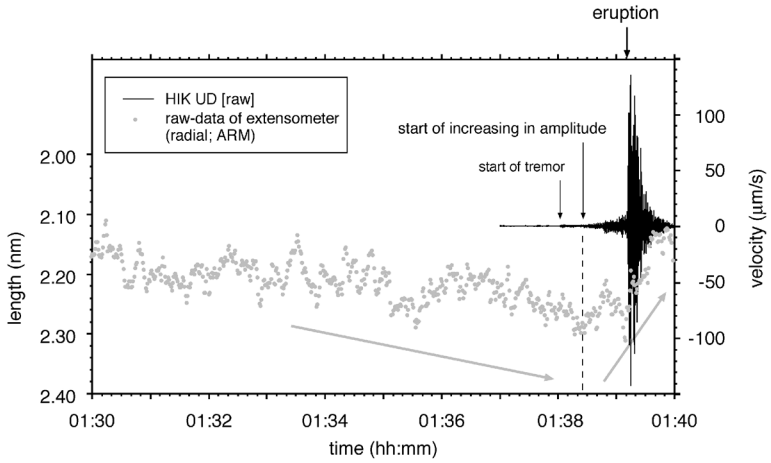

Fig. 7. Comparisons of the vertical component of seismic velocity at HIK and raw extensometer data at ARM (radial component) for the eruption on September 27, 2009. About 1.5 min prior to the onset of the eruption, a small tremor occurred, then growing in amplitude (vertical dashed line). The time of the start of the increase in amplitude in the tremor signal seems to correspond to the turning time of the strain data trend (thick arrows along with the data).

eruption, representing the nighttime background value on the surface of the volcano flank. It suddenly increased to 240 at the onset of the eruption (02:59) because of the dispersion of incandescent ejecta around the crater. It then dropped back to the previous background value of ～140 in about 10 min as the ejected materials cooled down. The period of the glow disappearance apparently corresponded to the 2nd stage of the strain record (Fig. 4a).

Infrared movies

We compared the infrared thermal movies taken at KUR with the raw extensometer data measured at ARM. Fig. 9a shows the temporal variations in the apparent temperature just above the crater prior to and after the 04 : 32 eruption on December 29, 2009. Although we can see the change in average temperature is almost stable at ～10℃ for the 10 min prior to the eruption in the upper diagram of Fig. 9a, at around 04:31:30, the temperature increased slightly by ～2℃ approaching the time of eruption (lower diagram). Interestingly, the onset time of the temperature increase coincides with the onset of the 3rd stage of the strain record (lower diagram). However, there is no large difference in the thermal images I and II (Fig. 9b) nor in the visible movies. Because pure hot gas has a very low emissivity (＜0.2) and it is not visible theoretically on the thermal image, this indicates that hot gas with vapor and much smaller amount of ashes started being exhausted at

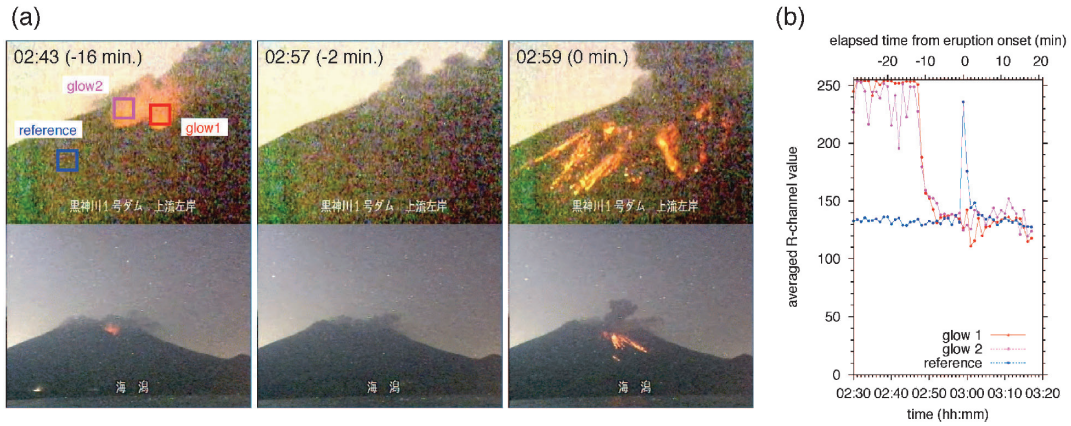

Fig. 8. (a) Sequential nighttime images on August 27, 2009, captured from movies taken by two high-sensitivity cameras deployed around Sakurajima (upper: KRL and lower: KAI; Fig. 1a). Small square regions of 20×20 pixels in the first picture are selected for evaluating the temporal change of the glow strengths. (b) Temporal change of averaged R-channel values in three small selected regions in (a).

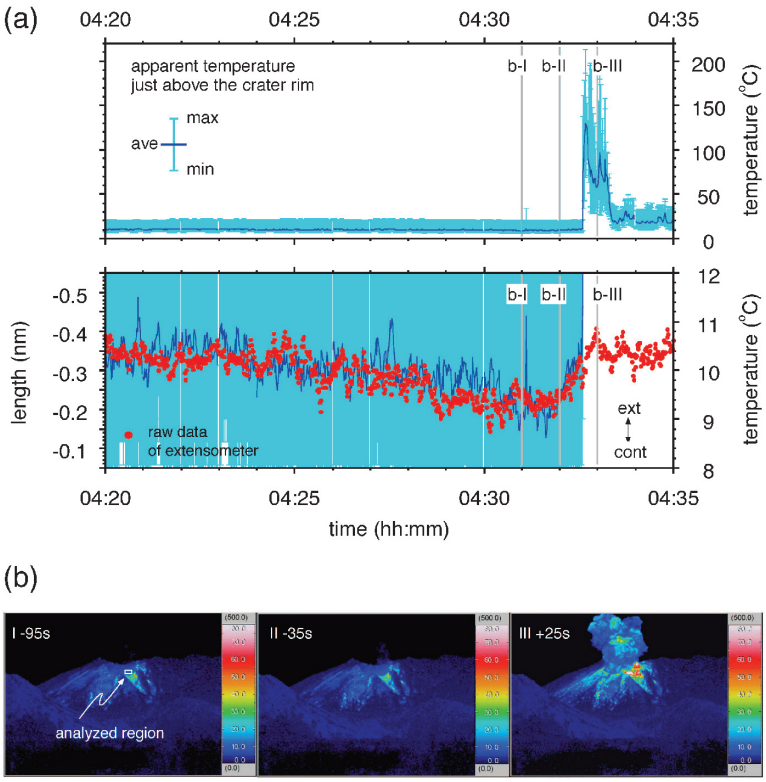

Fig. 9. (a) Temporal variations in apparent temperature above the crater (max./min.: light blue, average: blue) and raw data of the ARM extensometer (radial component: red dots) for the eruption on December 29, 2009. The region analyzed for the extraction of the temperature (10×5 pixels) is depicted by a white box in (b). The times when the trends change in both data sets are synchronized at about 1 min prior to the onset of an eruption (lower diagram). (b) Thermal snapshots of (I) 95 s before, (II) 35 s before, and (III) 25 s after the onset of eruption, respectively, taken from KUR.

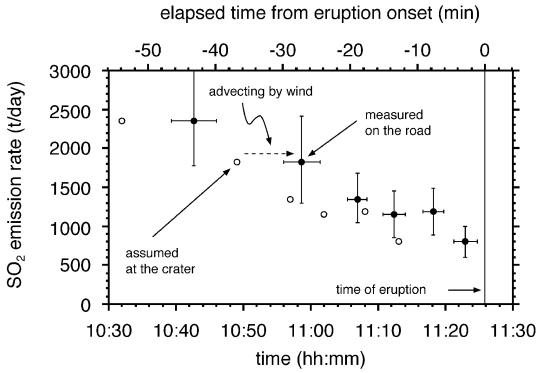

Fig. 10. Traverse DOAS data prior to the 11 : 25 eruption on February 6, 2008 (see also Fig. 12). Measured data are shown by solid symbols and time-corrected data considering advection by the wind (13 m/s) are shown by open symbols. Horizontal and vertical bars on the measured data show times for each traverse trace and ±25 % of measured SO_2 values, respectively.

the same time as the ground deformation changed.

SO_2 release

The timing of the increase in the strain rate (start of the 2nd stage) may correspond with the decrease in the release of volcanic gas. Changes in the SO_2 discharge rate were occasionally observed during DOAS measurements on the same time scale as other phenomena preceding eruptions in a few tens of minutes to a few minutes prior to the eruption. Fig. 10 shows an example in which there is a clear decrease trend in the gas discharge rate, more or less, 30 min prior to the eruption. The SO_2 discharge dropped from 2500 t/day to 1000 t/day, even although we cannot strictly identify the onset using DOAS data as the first traverse took place from 10:40−10:46. A drop in the SO_2 release about 20 min prior to an eruption at Sakurajima was also measured directly by a UV camera system in December 2009 (Kazahaya and Mori, 2010).

4−2 At time of eruption

Seismograms

Yokoo and Tameguri (2009) analyzed 81 explosion earthquakes of the 2008 Showa crater eruptions recorded at the HAR station (Fig. 1a) and found three characteristic phases in the first three seconds of the earthquakes (the first two columns in Fig 11). The first part consists of the P-wave first motion produced in a deeper location of the volcano. The particle motion of this phase plotted on the vertical-radial motions plane (Yokoo and Tameguri, 2009) is quite similar to that of the P-phase of explosion earthquakes associated with eruptions from the summit crater; thus, relatively the same source depth (about 2 km below the crater) of the summit explosion could be assumed for the Showa crater eruptions. The second phase, showing a retrograde rotation on the vertical-radial plane, though, had not been observed in the summit crater eruptions. The apparent travel speed of this phase is almost the same as the first P-wave, but the duration of this phase seems to become longer as the distance increases. These facts suggest that this phase mainly consists of Rayleigh wave. The third phase is also composed of Rayleigh waves, in the same manner as in the LP phase of explosion earthquakes of the summit eruptions (Tameguri *et al.*, 2002). These results suggest that similar mechanisms are at work in Showa crater eruptions as the summit crater eruptions (Temeguri *et al*., 2002) although the cause producing the observed second phase are not surely unknown yet; different source mechanism or the effect of the structures through which the waves propagate.

Infrasound

We also observed a somewhat complicated set of infrasound waveforms as well as the seismograms (Yokoo and Tameguri, 2009). The last two columns of Fig. 11 show four examples of infrasound waves recorded in 2009 that show a wide variation during the phase preceding the large amplitude onset of the shock-like main phase. Fig. 11a and 11b, respectively, are without and with the "preceding phase" (Yokoo *et al*., 2009), that is a weak and slow pressure increase. Fig. 11c and 11d are, respectively, an example in which an increase in pressure started slowly —in a similar way to the normal preceding phase —but then stopped due to the stagnation: and an example, with a pulse-like pressure change. The duration of the preceding phase (the time difference from the onset of a preceding pressure change to the onset of the main phase) has a negative relation with the amplitude of the main phase (Yokoo and Tameguri, 2009). The arrival time difference between the preceding infrasound phase at ARM and the third seismic wave (LP) phase at HAR is almost constant at about 4.5 s, regardless of how the type of preceding phase varies. During the eruptions without an infrasound preceding phase (Fig. 11a), the 4.5 s differences were also observed for the arrival times of the infrasound main phase at ARM and the seismic third LP phase at HAR. This time approximately equals the travel time difference between infrasound wave from the crater to ARM and seismic wave from the crater to HAR, of 6.8 s and 2.3 s, respectively.

Video records

The sequence of surface phenomena for the explosive eruption at the Showa crater at 11:25 on February 6, 2008 is shown in Fig. 12, as a typical example. Prior to the onset of the eruption, there was only a diluted volcanic gas steam was emitted from the crater. At 11:25:55, a main shock-like infrasound wave (Yokoo *et al*., 2009) suddenly occurred, followed by a dense volcanic cloud. The formation of an instantaneous condensation cloud (phase change of H_2O in the air from vapor to steam) occurred by adiabatic expansion and cooling due to the passage of the rarefaction phase of such a strong infrasound wave, which was clearly recognizable above the crater for a short

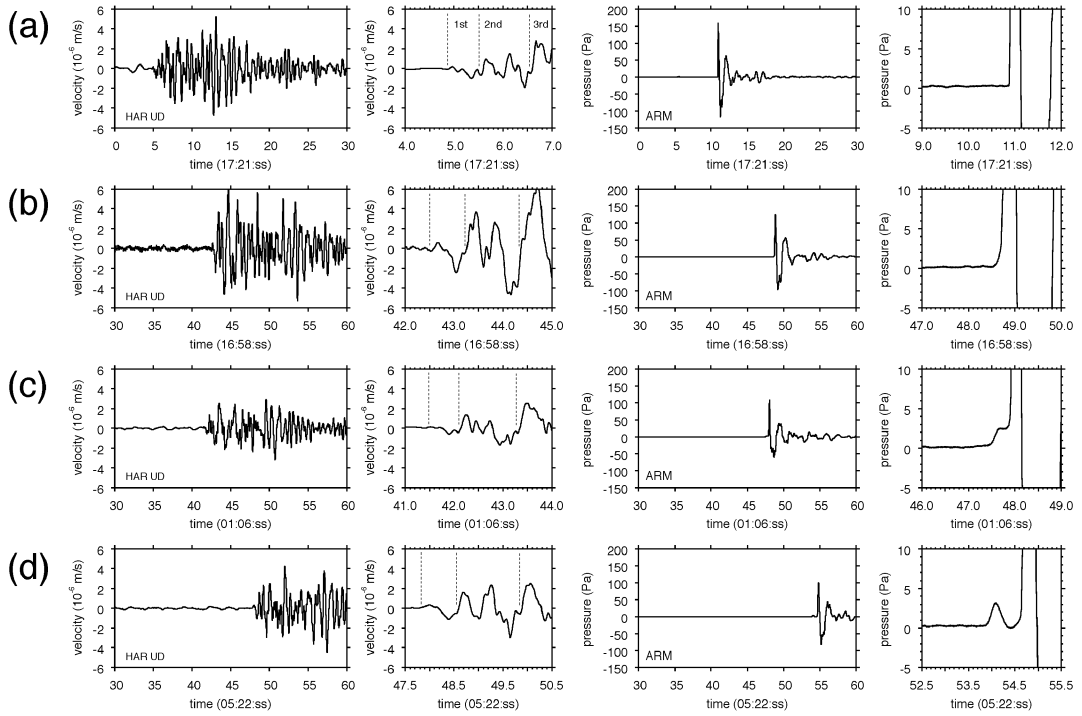

Fig. 11. Seismic and infrasound waveforms for the Showa crater eruptions observed at HAR (first two columns on the left) and ARM (on the right), respectively. Events at (a) 17 : 21 on February 3, (b) 16 : 58 on April 2, (c) 01 : 06 on March 10, and (d) 05 : 22 on March 10, 2009. The right-hand images are close-up waveforms of each initial part with a fixed time window of 3 sec. Labels marked 1st, 2nd, and 3rd indicate the phases as determined by Yokoo and Tameguri (2009).

period. A volcanic cloud contains numerous volcanic bombs, but it is not easy to see them during daytime eruptions, in contrast to the nighttime eruptions in which many incandescent bombs are clearly recognizable preceding the volcanic cloud (Fig. 12f).

5. Discussion

5−1 Magma migration and storage

The strain change in the 1st stage is considered to be pressurization induced by magma migration within the volcano, which is a view proposed for the summit crater eruptions (Ishihara, 1990; Iguchi *et al*., 2010).

In the summit crater eruptions (Ishihara, 1990), both radial and tangential strains were extensions, and the tilt was crater-side-up prior to the eruptions, and both were inverted during the eruption. The deformation pattern in the Showa crater eruptions is similar to that in the summit eruptions in terms of the strain change, which is inverted during eruptions, although only the tangential strain is extensional while the radial component is in contraction (Figs. 3 and 5). This difference can be explained by different source depths. The radial-to-tangential strain ratio ($\beta = \varepsilon_r/\varepsilon_\tau$) and the distance from the source to the station r are related to the source depth d in the most simple way by an inflating sphere in a homogeneous elastic half space (Mogi, 1958):

$$d = \sqrt{\frac{2+\beta}{1-\beta}} \times r.$$

In the summit eruptions, β was positive and the pressure source was estimated to be located 2−6 km beneath the volcano, with a suggested volume change of $10^3 - 10^6$ m^3 (Ishihara, 1990). On the other hand, in Showa crater eruptions, the negative β gives a smaller d. For example, the source of the 09:52 eruption on August 6, 2009 (Fig. 3) was estimated to be 1.2 km beneath the crater. The depths of almost all the explosions in the last half of the year 2009 range from 0 km to 2 km with a mean distribution around 1 km (Iguchi *et al*., 2010). This result suggests that the pressure for a Showa crater eruption is concentrated in a much shallower portion of the conduit than for the Sakurajima's main magma chamber, which is 2−6 km deep (Ishihara, 1990). This is a reason that the tilt prior to the eruption was small as same as the background variation (Fig. 3a). We, however, should note that neglecting topography in this simplest approximation could cause the depth of the pressure source to be overestimated (Williams and Wadge, 1998). The actual depth of the pressure

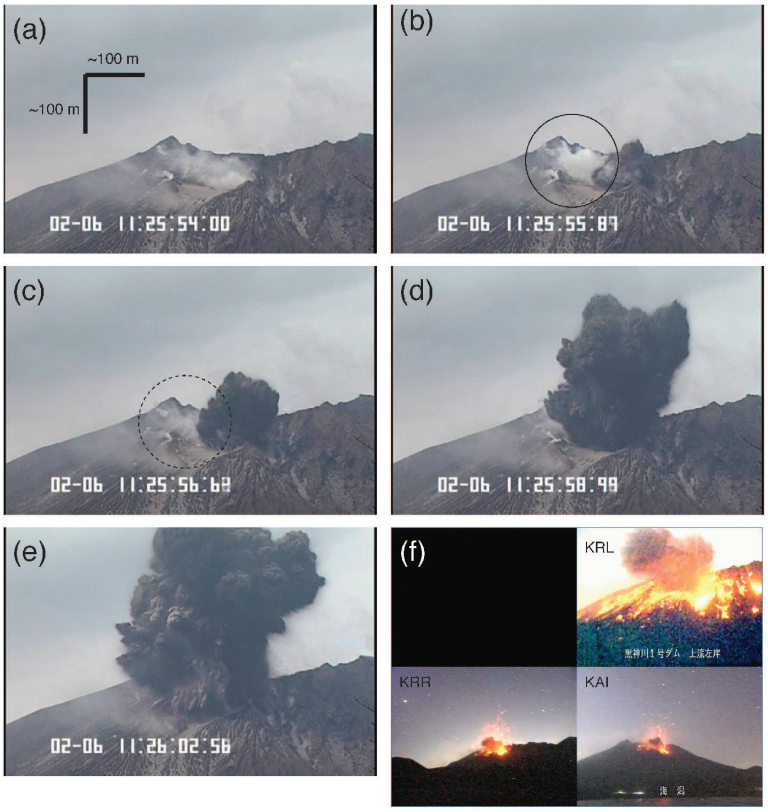

Fig. 12. (a–e) Screenshots of the 11 : 25 eruption on February 6, 2008, obtained by the movie system at KUR. The condensation cloud caused by the passage of a strong shock-like infrasound wave (rarefaction phase) shown by a circle in (b) has returned to its original appearance in (c), which resembles (a). (d–e) Outburst growing volcanic cloud with numerous ballistic bombs at the head of the cloud. (f) Typical image of a nighttime eruption (23 : 18 on October 14, 2009). The three letters on each image are the names of the MLIT camera sites (Fig. 1a).

source preceding the eruption may be far shallower than the estimated value.

During summit eruptions in 1990s, small earthquakes with peak frequencies in the 3–8 Hz band, classified as BH-type earthquakes, occurred 2. 5–3. 5 km beneath the crater in association with ground inflation (Iguchi, 1995). Multitudes of small BH-type earthquakes have been argued to be produced by the migration process of magma moving into the lower part of a conduit. Because this magma migration leads to an accumulation of stress in the wall rock around the conduit, some brittle failures such as VT earthquakes were assumed to occur. This type of earthquake is also sometimes observed in the 1st stage of the Showa crater eruptions (Fig. 6).

On the other hand, we rarely observed LP (long-period) earthquakes with low peak frequencies of around 1–3 Hz ("BL-type earthquakes" in Sakurajima; Iguchi, 1995) during this inflation period associated with Showa crater eruptions. The BL-type earthquakes are tied to volumetric expansion caused by the formation of bubbles within the magma (Iguchi, 1995). One speculative explanation for the absence of BL-type earthquakes in Showa crater eruptions would be that no effective bubble formation occurs during this stage because intruding magma maintains relatively high pressures within the conduit due to the higher ascension speed of the magma than for the summit eruptions.

As described above, it is thought that the ground deformation associated with BH-type earthquakes in the 1st stage of the strain change is produced by magma migration in a volcano to a shallow location of about 1 km deep. However, in some cases, ground inflation ceases and stagnates without any kind of surface phenomenon as observed during the summit eruptions (Tateo and Iguchi, 2009), *e.g.*, ejection of volcanic materials. This means that the stagnation period of the strain change prior to the eruption is not due to a balance between the input and the output of the mass of magma through the crater. The intrusion of magma stopped and it stayed in situ more or less in a stable condition. In other words, there would

already be a cap covering the crater that would bear down on the magma in the conduit to prevent an eruption. For that matter, we posit that the pressure accumulation process caused by magma intrusion occurs in preparation for the next eruption, but it is not the process that triggers the onset of eruption itself, as an increase in pressure alone is not sufficient to lead to an immediate eruption. The mechanism that directly triggers the eruption, releasing the intruded magma, is considered to be another phenomenon.

5−2 Crater bottom sealing process and formation of gas pocket

The 2nd stage is defined by the increase in the strain change (Fig. 4). Because the change overlapping the strain trend has the same characteristics as the 1st stage strain change (radial contraction and tangential extension), it is inferred that the ground deformation in this stage includes an additional inflation source at a shallow depth.

An important observation is that a volcanic glow weakens and then disappears at the beginning of the strain 2nd stage (Fig. 8). It is considered that the crater glow observed at night is simple evidence of the presence of incandescent high-temperature materials in the shallow portion of the crater (Yokoo, 2009), like a lava dome/pond. The weakening and disappearance of the volcanic glow indicates either the sealing of a shallow conduit and the cooling of incandescent rocks (or molten lava) inside the crater, nor a deepening of the magma level in the conduit. However, the latter possibility can not explain the additional inflation source, thus rejected here. Besides, it has been reported that the SO_2 discharge rate as measured with a UV camera gradually decreases for 20 min prior to an eruption (Kazahaya and Mori, 2010), that is same time range as for the 2nd strain stage. The decrease in gas release can also be explained by the process of the sealing of the gas pathway in the shallower portion of the conduit. The heat supplied by the volcanic gas into the atmosphere decreases and eventually ceases, which explains the gradual decrease of the apparent temperature above the crater observed in the infrared images (Fig. 9a). A decrease in the thermal radiance of the crater walls has also been observed at Stromboli 1 hour before the violent explosive paroxysm of April 5, 2003 (Ripepe and Harris, 2008).

Details of the sealing process that occurs at the Showa crater are still poorly understood. However, recent experiments (Otsuki and Nakamura, 2012) may be used to explain the processes in the 2nd stage. They have demonstrated that a permeable melt foam with deformed bubbles may change into a melt with isolated spherical bubbles due to the surface tension of a melt in a relatively short time (<30 minutes), which suggests that this can result in the formation of impermeable lava caps in the crater in the same time scale. As this kind of sealing process proceeds, gas consequently accumulates in the uppermost part of the conduit, which is plugged by an impermeable magma that is cooling. This leads to the formation of a gas pocket beneath the plug, which generates an overpressure, detected as an inflating deformation signal.

We can also estimate the source pressure of the gas pocket using these overlapping strain data, assuming the source is a sphere of 10 m radius and 10^9 Pa for Lame's coefficient in the Mogi model (Mogi, 1958), to be 0.5×10^7 to 7×10^7 Pa. These pressures are almost the same order but slightly higher than relatively larger examples of the summit explosions estimated by a shock-tube model, 1.4×10^7 to 2.8×10^7 Pa (Ishihara, 1985). If the source size is 3×10^4 m^3 equivalent to a cylinder with a 100 m length and a 10 m radius, the source pressure becomes one-order lower value, 1×10^6 to 9×10^6 Pa, which sounds reasonable in terms of the small scale of Showa crater eruptions (Iguchi *et al*, 2010).

Processes similar to those in the 2nd stage of the strain change at Sakurajima have been observed in other volcanoes (*e.g.*, Ripepe and Harris, 2008; Genco and Ripepe, 2010; Bonaccorso *et al.*, 2012), but in different time scales. Hirabayashi *et al*. (2005, 2007) detected a decrease in the discharge rate of SO_2, 3 min prior to explosions at the Suwanosejima and Semeru volcanoes. They interpreted this as gas entrapment below the cap beneath the crater, but without accounting for why the shallow part of the conduit seals to prevent gas escaping. Upward ground displacement and tilt indicating shallow inflation beneath the crater, have been detected 1−2 min and 3−30 min prior to the explosions at the Suwanosejima and Semeru volcanoes, respectively, and these inflation-related deformations are thought to represent the accumulation of volcanic gas in the upper part of the conduit (Iguchi *et al.*, 2008a).

At Asama volcano, which is an andesitic volcano whose activity closely resembles that of Sakurajima, the internal structure of the volcano was estimated by using the leading-edge Muon tomography method (Tanaka *et al.*, 2010). Tomography shows a region with low bulk density (0.8 ± 0.2 g/cm^3, implying a porosity of 25−45 %) beneath the crater floor covered by an extruded lava dome. This evidence is not directly comparable to the suggested gas pocket we infer as being formed below the crater floor of Sakurajima, but the presence of this lower-density region just beneath the dense lava plug at the vent is very important.

5−3 Gas and pressure leakage

Strain with radial contraction and tangential extension is inverted during the 3rd stage, a few minutes prior to eruptions (Fig. 5). The inverted trend of the strain record is interpreted as the pressure decreasing in the shallow portion of the volcano. Infrared movie observation shows a slight temperature increase above the crater during this stage (Fig. 9). The shallow decompression and the temperature increase could be produced by volcanic gases leaking from the gas pocket into the atmosphere.

A small-amplitude tremor with a 4 Hz spectral peak

emerged a few tens of seconds prior to the strain 3rd stage (Fig. 7). We assume that this tremor is produced by the fracturing of the magma lid because the accumulated gas pressure beneath the crater exceeded the threshold level of the strength of the material. The amplitude of tremor starts to grow at the time of the onset of the 3rd stage (vertical dashed line in Fig. 7). An amplitude increase might indicate an increase in the flow volume of the gas into the fractures, or the progression of the fracturing process.

The effect of the decompression of the gas pocket due to the gas leakage propagates deeper into the conduit. This thus induces the start of degassing from both dense and vesiculated magma in the mingling zone beneath the gas pocket. When the effective decrease in pressure reaches the head of the water-saturated dense magma body, it culminates in a sudden increase in the total volume of the mixture of (fragmented) magma and the exsolved gases. This expanding process may correspond to the onset of explosion earthquakes (Tameguri *et al.*, 2002). We can assume the relatively resemblance of the source depth of the Showa crater eruptions to the same as the case of the summit eruptions, about 2 km below the volcano (Tameguri *et al*., 2002), because the source direction inferred from the particle motion of the first phase of explosion earthquakes is similar (Yokoo and Tameguri, 2009). Considering this seems slightly deeper than the depth of pressure accumulation, around 1 km on average, estimated from the strain record, it may be necessary to determine details of the source processes and depths by a more precise analysis of explosion earthquakes.

5−4 Failure of the crater ground

Upon the sudden out-gassing and fragmentation of the magma, a pressure wave is radiated toward the surface in the conduit (Tameguri *et al.*, 2002; Iguchi *et al.*, 2008a). At the same time, the expanding mixture of magma and gases moves upward. This induces a lower confining pressure of the mixture responsible for the exsolution of the water from the magma as they migrate upward. The total volume of mixtures, then, increases.

When the mixture of fragmented magma and exsolved gases reaches the shallower gas pocket, the sealing plug starts to swell to failure, as proposed by Yokoo *et al*. (2009) based on the results that the shallow expansion phase (LP phase) of the explosion earthquake and the preceding phase of infrasound wave were produced at almost the same time (Yokoo and Tameguri, 2009). The upward motion of the plug surface is considered to be represented by the infrasound preceding phase. The upheaval volume of the plug just before bursting, but during the time of radiating preceding infrasound, is estimated from its waveform to be around 250 m^3 for the 11:25 eruption on February 6, 2008, based on Yokoo *et al*. (2009). This is the largest value in the past three years. Almost all cases are less than 100 m^3. These values are about the same size as for the eruption at Suwanosejima volcano (Yokoo and Iguchi, 2010), which suggests that the vent size of the Showa crater is much smaller than that of the summit crater (～20 m; Ishihara, 1990). This was confirmed by aerial photographs taken in May 2011 by the Japan Meteorological Agency, as being ～5 m. However, this 5 m is half the size of the pressure source we assumed in the previous section (10 m radius of a cylinder with a 100 m thick). It suggests that size of the conduit would taper near the surface.

When the plug fails, the strong main phase of an infrasound wave is radiated together with the release of mixtures of high-pressurized expanding gas and magma fragments (Figs. 11 and 12). At the summit eruptions, Tameguri *et al*. (2002) found that the amplitude of the LP phase of an explosion earthquake and that of the main phase of infrasound waves are positively related: however, no such good correlation is seen in the Showa crater eruptions (Iguchi *et al*., 2010). The amplitude of the main phase of infrasound was compared with the duration of the strain 3rd stage, during which the gas pocket was considered to be formed, but no clear correlation was seen (Fig. 13a). The amplitude of the main phase of infrasound also has almost no positive correlation to the amplitude of the strain changes during the 2nd stage (Fig. 13b). These two results mean that accumulated gas in the gas pocket, which induces acceleration in the strain change in apparently the 2nd stage, is not directly related to the intensity of the radiation of the main phase of infrasound wave. Which parameters control the intensity of the infrasound radiation? An additional observed fact, the negative relation of the amplitude to the duration of the preceding phase (Yokoo and Tameguri, 2009), may have to be considered. The deformation process of the lid will become a good indicator in accounting for the observed amplitude of the main phase, which is suggested by an experimental approach of a bubble bursting (Kobayashi *et al.*, 2010).

5−5 Time sequence of Showa crater eruptions

The time series of recorded signals and their characteristics as obtained from our multi-parametric geophysical observations are very instructive in understanding the eruption processes at the Showa crater of Sakurajima volcano. Here, we summarize the processes preceding the onset of an eruption as shown in Fig. 14, focusing in particular on the processes forming and destroying a gas pocket beneath the crater.

A few hours prior to the onset of an eruption, magma starts to migrate and be stored at depths of around 0−2 km (Fig. 14a). This is clearly recognizable in the record of strain change as an inflation process. Starting a few tens of minutes prior to the eruption, the SO_2 gas emission rate gradually decreases, indicating that a sealing process is progressing at the crater bottom as the eruption approaches (Fig. 14b). A few tens of minutes to a few minutes prior to the eruption, the rate at which the volcano is inflating starts

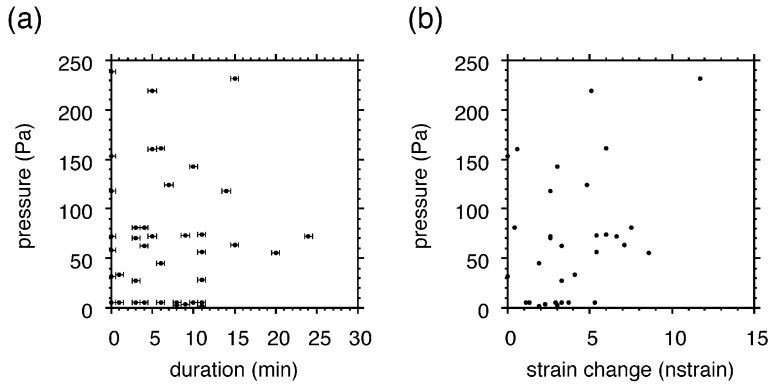

Fig. 13. (a) Relationship between periods of the 2nd stage of strain change when the volcanic glow disappears just prior to the onset of an eruption, as identified on the MLIT video network, and the excess pressure of infrasound waves at ARM (40 nighttime events from August 2009 to January 2010). (b) Excess infrasound pressures corresponding to inflating amplitudes at ARM's radial strain (32 events from August to December 2009).

to accelerate due to the construction of a plug at the magma surface, which causes the formation of a gas pocket beneath the crater (Fig. 14c). This process is also observed as the weakening and then disappearance of a volcanic glow during nighttime events. A few minutes prior to the eruption, a small tremor starts to emerge (Fig. 14d). Its amplitude grows, and the inflating strain changes to a deflating process. This is thought to occur as gas is released through newly formed fractures within the plug. Seismic signals show that dynamic processes resembling the eruptions at the summit crater also occur during Showa crater eruptions (Fig. 14e). Expanding magma then rises and pushes the gas pocket up, which leads to a swelling of the crater ground, and a phase of radiating weak infrasound waves. After the failure of the plug due to its deformation, the accumulated gasses and expanding magma itself are ejected together from the crater, following the ejection of volcanic bombs at the start of the eruption's surface phenomena (Fig. 14f).

The model described in this paper still contains much speculation, especially in the process relating to the shallow decompression due to leakage, explosion earthquakes at depth, and the swelling and failure of the plug. We think these processes will become important clues for a better understanding of the Showa crater eruptions. However, these subjects are left for a future work because the main aim of this paper is to present observed evidences related to the formation of a gas pocket within a time scale.

6. Conclusions

From our multi-parametric observations at Sakurajima volcano, Japan, typical processes that occur prior to the outburst of explosive eruptions at Showa crater have been revealed and the following conclusions were reached:

(1) Magma starts to migrate to a depth of 0−2 km beneath the crater and is stored there for a few hours prior to eruption. This is clearly identifiable in strain records with both radial contraction and tangential extension changes. This magma intrusion induces the occurrence of small earthquakes around the conduit.

(2) A few tens of minutes to a few minutes prior to eruption, a decrease in the SO_2 discharge rate and an acceleration of volcano inflation are observed. During nighttime eruptions, a weakening and then disappearance of the volcanic glow is seen. This is due to the formation of a gas pocket sealed by a consolidating lava plug beneath the crater.

(3) Once the gas amassed in the gas pocked attains sufficient pressure to overcome the threshold value for deforming the lid, fracturization occurs within the plug, so minor amounts of gas and pressure leak from the gas pocket into the atmosphere. This induces volcano contraction and produces small tremors a few minutes prior to the onset of an eruption.

(4) An explosive eruption, accompanied by the radiation of infrasound waves, follows the explosion earthquake at the Showa crater as well as in the case of summit crater eruptions at Sakurajima volcano. However, not all of the source mechanisms are described in this paper due to lack of data, so further work should be done in the future.

Acknowledgments

We are grateful to all the members of the Sakurajima Volcanological Observatory for their support of our research. Geophysical observations carried out at ARM were performed as collaborative work by Osumi Kasen Kokudo Jimusho, MLIT, and SVRC, DPRI of Kyoto University. M. Ichihara, two anonymous reviewers, and the editor T. Nishimura are greatly acknowledged for their comments that improved the quality of this paper. This research is

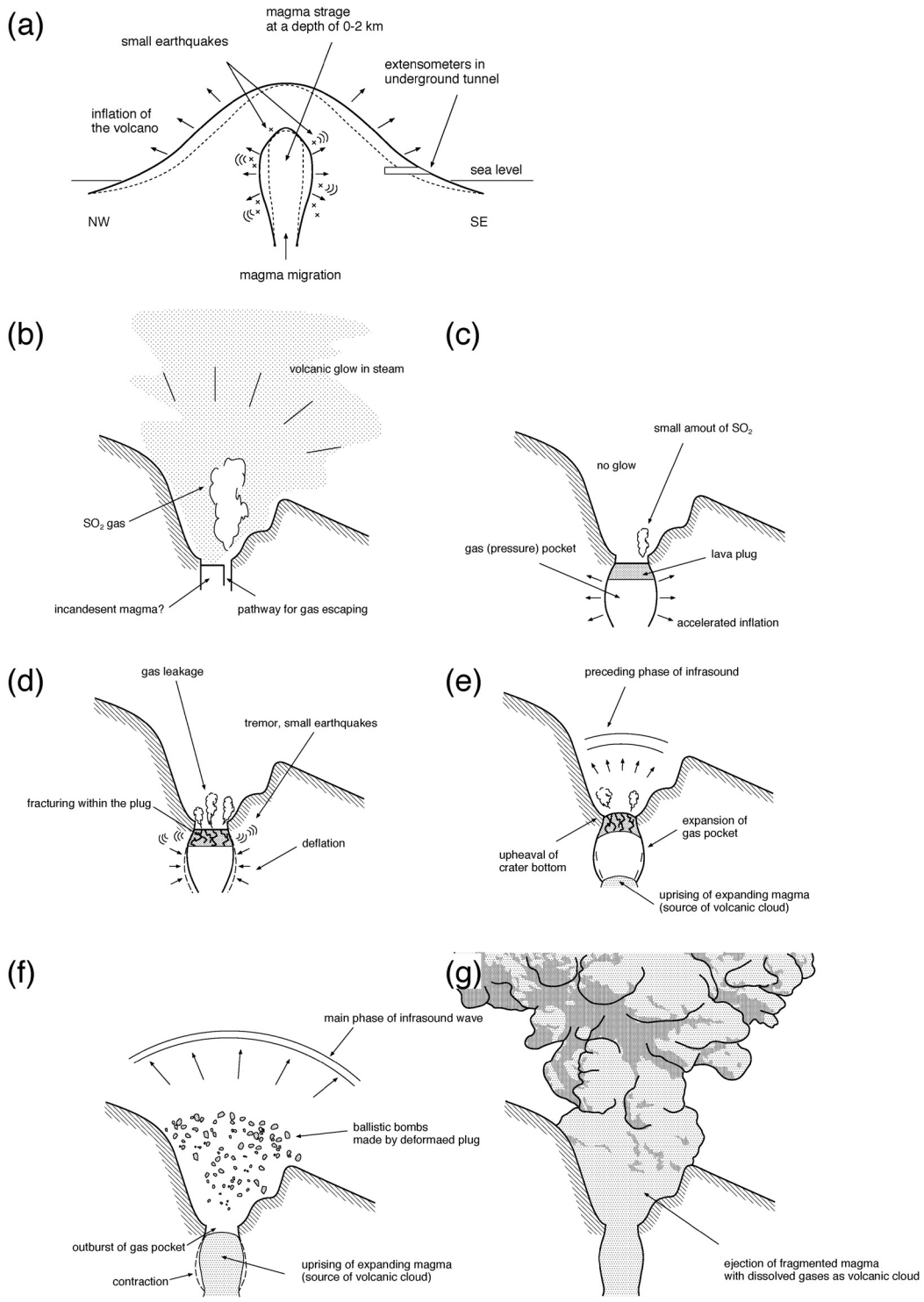

Fig. 14. Sequential schematic images of processes occurring prior to the onset of an eruption. (a) A few hours prior to eruption. (b-c) A few tens of minutes to a few minutes prior to eruption. (d) A few minutes prior to eruption. (e) Half a second prior to eruption. (e) Onset of an eruption. (g) After the onset of an eruption. Vertical and horizontal scales in these images are not shown. See text for details.

partially supported by JSPS Research Fellowship AY (No. 19·126) and Tohoku University's GCOE program "Global Education and Research Center for Earth and Planetary Dynamics" (PI: E. Ohtani).

Appendix: Fluctuations in ground deformation record

Differing from the obvious ground deformations caused by magma migration, strain fluctuations of only a few nano-strains are clearly recognizable in all strain change records. We considered the meaning of these small perturbations by comparing them with eruptive surface phenomena. Average luminance data for two regions at the crater and an area nearby are extracted to retrieve the time sequence of the surface phenomenon.

By this method, eruptions with ash venting are clearly identified by the peaky negative changes in the differences of average luminance in these two regions (Figs. A1a and A1b). A set of oppositely directed strain change patterns in the radial and tangential components at ARM are almost always observed during these periods of ash venting (Fig. A1c). This indicates that ejection of ashes and gases doubtlessly causes a release of pressure from the volcano, inducing small changes in the strain record.

However, many fluctuations with the same order of amplitude as ash emissions are also observed without significant surface phenomenon occurring, such as in the period prior to the eruption (08 : 00–09 : 40 on September 18, 2009). This means that these small changes are occasionally affected by certain processes occurring within the volcano. Small fluctuations might be caused by a process of pressure recovery due to the depressurization of the magma conduit (*e.g.*, ascending magma; Nishimura, 2004). It is, therefore, difficult to distinguish why such small strain changes (of the order of few nano-strains) may be eruptive or non-eruptive without surface observations (the process works only underground). It should be noted that peaky changes in luminance around the period from 08:40 to 09:25 (Fig. A1a) were caused by a dappled shade from clouds.

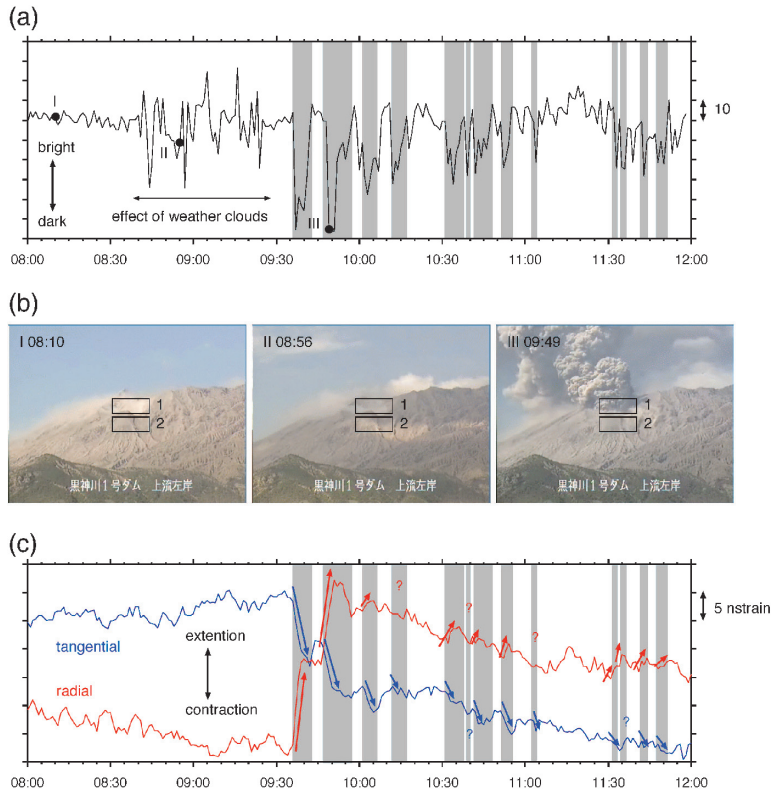

Fig. A1. (a) Difference in luminance between two selected regions in the movie image (1 and 2 in (b)) on September 18, 2009. Higher value of the difference means brightening in the crater area. The shaded periods denote times of ash venting, thus lower luminance values are calculated. Times denoted by dots at (I) 08 : 10, (II) 08 : 56, and (III) 09 : 49 correspond to the images in (b). (b) Images taken by camera at KRL (Fig. 1a). Two regions, the crater (1) and the reference region (2), are for evaluating changes in luminance. The size of each region is 50 × 20 pixels. (c) Strain changes in each component at ARM during these times.

References

Bonaccorso, A., Clavari, S., Linde, A., Sacks, S. and Boschi, E. (2012) Dynamics of the shallow plumbing system investigated from borehole strainmeters and cameras during the 15 March, 2007 Vulcanian paroxysm at Stromboli volcano. *Earth Planet. Sci. Lett.*, **357−358**, 249−256, doi: 10.1016/j.epsl.2012.09.009.

Burgisser, A., Arbaret, L., Druitt, T. H. and Giachetti, T. (2011) Pre-explosive conduit conditions of the 1997 Vulcanian explosions at Soufrière Hills Volcano, Montserrat: II. Overpressure and depth distributions. *J. Volcanol. Geotherm. Res.*, **199**, 193−205, doi: 10.1016/j.jvolgeores.2010.11.014.

Calvari, S., Inguaggitato, S., Puglisi, G., Ripepe, M. and Rosi, M. (2008) The Stromboli Volcano: An integrated study of the 2002−2003 eruption. *Geophysical Monograph 182*, American Geophysical Union, Washington, DC., pp. 399.

Genco, R. and Ripepe, M. (2010) Inflation-deflation cycles revealed by tilt and seismic records at Stromboli volcano. *Geophy. Res. Lett.*, **37**, L12302, doi: 10.1029/2010GL042925.

Gottsmann, J., De Angelis, S., Fournier, N., Camp., M. V., Sacks, S., Linde, A. and Ripepe, M. (2011) On the geophysical fingerprint of Vulcanian explosions, *Earth Planets. Sci. Lett.*, **306**, 98−104, doi: 10.1016/j.epsl.2011.03.035.

Hirabayashi, J., Oikawa, J., Iguchi, M., Mori, T. and Shinohara, H. (2005) Volcanic explosion and accumulation of volcanic gases at Suwanosejima volcanoes. *Dynamics of Volcanic Explosion*, **3**, 45−48 (in Japanese).

Hirabayashi, J., Oikawa, J., Onizawa, S., Mori, T. and Iguchi, M. (2007) Discharge rate of volcanic gases and volcanic explosions− Suwanosejima and Semeru volcanoes. *Dynamics of Volcanic Explosion*, **5**, 70−74 (in Japanese).

Iguchi, M. (1995) A vertical expansion source model for the mechanisms of earthquakes originated in the magma conduit of an andesitic volcano: Sakurajima, Japan. *Bull. Volcanol. Soc. Japan*, **39**, 49−67.

Iguchi, M., Yakiwara, H., Tameguri, T., Hendrasto, M. and Hirabayashi, J. (2008a) Mechanism of explosive eruption revealed by geophysical observations at the Sakurajima, Suwanosejima and Semeru volcanoes. *J. Volcanol. Geotherm. Res.*, **178**, 1−9, doi: 10.1016/j.jvolgeores.2007.10.010.

Iguchi, M., Yokoo, A. and Tameguri, T. (2008b) Characteristics of ground deformation associated with eruptions at Showa crater, Sakurajima volcano. *Abstr. Volcanol. Soc. Japan 2008 Fall Meet.*, B26 (in Japanese).

Iguchi, M., Yokoo, A. and Tameguri, T. (2010) Intensity of volcanic explosions at Showa Crater of Sakurajima Volcano. *Annuals of Disas. Prev. Res. Inst., Kyoto Univ.*, **53B**, 233−240 (in Japanese with English Abstract).

Ishihara, K. (1985) Dynamical analysis of volcanic explosion, *J. Geodyn.*, **3**, 327−349, doi: 10.1016/0264−3707(85)90041−9.

Ishihara, K. (1990) Pressure sources and induced ground deformation associated with explosive eruptions at an andesitic volcano: Sakurajima volcano, Japan. In *Magma Transport and Storage* (Ryan, M. ed.), Wiley, New York, 335−356.

Ishihara, K. (2000) Characteristics and conditions of vulcanian eruptions. *Chikyu*, **22**, 308−314 (in Japanese).

Kamo, K. and Ishihara, K. (1989) A preliminary experiment on automated judgement of the stages of eruptive activity using tiltmeter records at Sakurajima, Japan. In *Volcanic Hazards: Assessment Methods and Monitoring*, Latter, J.H. ed., Springer Verlag, Heidelberg, 585−598.

Kazahaya, R. and Mori, T. (2010) Degassing activity fluctuation before eruptions at Sakurajima volcano, Japan, *Abstr. Cities on Volcanoes 6*, 1.3-O-13.

Kobayashi, T., Namiki, A. and Sumita, I. (2010) Excitation of airwaves caused by bubble bursting in a cylindrical conduit: Experiments and a model. *J. Geophys. Res.*, **115**, B10201, doi: 10.1029/2009JB006828.

Lyons, J.J., Waite, G.P., Ichihara, M. and Lees, J.M. (2012) Tilt prior to explosions and the effect of topography on ultra-long-period seismic records at Fuego volcano, Guatemala. *Geophy. Res. Lett.*, **39**, L08305, doi: 10.1029/2012GL051184.

Mogi, K. (1958) Relations between the eruptions of various volcanoes and the deformations of the ground surfaces around them. *Bull. Earthq. Res. Inst.*, **36**, 99−134.

Mori, T., Hirabayashi, J., Kazahaya, K., Mori, T., Ohwada, M., Miyashita, M., Iino, H. and Nakahori, Y. (2007) A compact ultraviolet spectrometer system (COMPUSS) for monitoring volcanic SO_2 emission: Validation and preliminary observation. *Bull. Volcanol. Soc. Japan*, **52**, 105−112.

Nishimura, T. (2004) Pressure recovery in magma due to bubble growth. *Geophys. Res. Lett.*, **31**, L12613, doi: 10.1029/2004GL019810.

Otsuki, S. and Nakamura, M. (2012) Experimental study on the textual relaxation of melt foam. *Abstr. JPGU Meeting 2012*, SVC54-P04.

Ripepe, M. and Harris, A.J.L. (2008) Dynamics of the 5 April 2003 explosive paroxysm observed at Stromboli by a near-vent thermal, seismic and infrasonic array. *Geophys. Res. Lett.*, **35**, L07306, doi: 10.1029/2007GL032533.

Tanaka, H.K.M., Uchida, T., Tanaka, M., Shinohara, H. and Taira, H. (2010) Development of a portable assembly-type cosmic-ray muon module for measuring the density structure of a column of magma. *Earth, Planets Space*, **62**, 119−129.

Tameguri, T., Iguchi, M. and Ishihara, K. (2002) Mechanism of explosive eruptions from moment tensor analyses of explosion earthquakes at Sakurajima volcano, Japan. *Bull. Volcanol. Soc. Japan*, **47**, 197−215.

Tamura, Y., Sato, T., Ooe, M. and Ishiguro, M. (1991) A procedure for tidal analysis with a Bayesian information criterion. *Geophys. J. Int.*, **104**, 507−516, doi: 10.1111/j.1365−246X.1991.tb05697.x.

Tateo, Y. and Iguchi, M. (2009) Ground deformation associated with BL-type earthquake swarms at Sakurajima volcano. *Bull. Volcanol. Soc. Japan*, **54**, 175−186 (in Japanese with English Abstract).

Turcottte, D.L., Ockendon, H., Ockendon, J.R. and Cowley, S.

J. (1990) A mathematical model of vulcanian eruptions. *Geophys. J. Int.*, **103**, 211–217, doi: 10.1111/j.1365–240X.1990.tb01763.x.

Voight, B. and Sparks, R.S.J. (2010) Introduction to special section on the Eruption of Soufrière Hills Volcano, Montserrat, the CALIPSO Project, and the SEA-CALIPSO Arc-Crust imaging experiment. *Geophys. Res. Lett.,* **37**, L00E23, doi: 10.1029/2010GL044254.

Williams, C.A. and Wadge, G. (1998) The effects of topography on magma chamber deformation models: Application to Mt. Etna and rader interferometry. *Geophys. Res. Lett.*, **25**, 1549–1552.

Yokoo, A. (2009) Continuous thermal monitoring of the 2008 eruptions at Showa crater of Sakurajima volcano, Japan. *Earth, Planets Space*, **61**, 1345–1350.

Yokoo, A. and Tameguri, T. (2009) Characteristics of infrasound and seismic signals associated with eruptions at Showa crater of Sakurajima volcano. *Annuals of Disas. Prev. Res. Inst., Kyoto Univ.*, **52**, 309–317 (in Japanese with English Abstract).

Yokoo, A. and Iguchi, M. (2010) Using infrasound waves from eruption video to explain ground deformation preceding the eruption of Suwanosejima volcano, Japan. *J. Volcanol. Geotherm. Res.*, **196**, 287–294, doi: 10.1016/j.jvolgeores.2010.08.008.

Yokoo, A., Iguchi, M. and Ishihara, K. (2007) Geothermal activity on the flank of Sakurajima volcano inferred from infrared thermal observation. *Bull. Volcanol. Soc. Japan*, **52**, 121–126 (in Japanese with English Abstract).

Yokoo, A., Tameguri, T. and Iguchi, M. (2009) Swelling of a lava plug associated with a Vulcanian eruption at Sakurajima Volcano, Japan, as revealed by infrasound record: case study of the eruption on January 2, 2007. *Bull. Volcanol.*, **71**, 619–630, doi: 10.1007/s00445–008–0247–5.

(Editorial handling Takeshi Nishimura)

桜島昭和火口におけるブルカノ式噴火の前駆プロセス

横尾亮彦・井口正人・為栗　健・山本圭吾

桜島において多項目地球物理観測を行い，昭和火口のブルカノ式噴火発生に至る一連のプロセスについて明らかにした．火口下 1 km の深さにマグマが貫入することによって，噴火の数時間前から山体が膨張する．噴火開始の数 10 分前には，火口底にプラグが形成されて脱ガス通路の閉塞が進行し，火口直下に火山ガスの溜まりが形成される．二酸化イオウ放出率の減少や山体膨張率の増加として観測されるほか，夜間であれば，火映が微弱化した後に消滅する．噴火数分前になると極小微動が起こり始める．プラグに亀裂が形成され，そこを通って火口底下に溜まっていたガスの放出が始まることに対応する．その後，放出されるガスが多くなることで，微動の振幅が大きくなる．山体膨張から収縮に転じ，火道内では小規模な減圧が誘引される．減圧の影響が水に飽和したマグマ深度まで到達すると，急激なマグマ発泡，破砕が始まり，爆発地震が発生する．破砕したマグマは火道内を上昇し，火口直下にあるガス溜まりを押し上げる．そのため，爆発地震の発生開始からおよそ 0.5 秒後には，ガス溜まりの上方にある火口底プラグが隆起して，空振先行相を励起する．プラグの変形が進行して破壊に至った後は，火道内を上昇してきた破砕マグマが火山噴煙として放出される．